New Insight into the Interaction between Propylene Carbonate-Based Electrolytes and Graphite Anode Material for Lithium Ion Batteries

Hong-Li Zhang, Cheng-Hua Sun, Feng Li, Chang Liu, Jun Tan, and Hui-Ming Cheng*

Shenyang National Laboratory for Materials Science, Institute of Metal Research, Chinese Academy of Sciences, 72 Wenhua Road, Shenyang 110016, China

Received: October 14, 2006; In Final Form: January 27, 2007

Sufficient understanding of surface chemistry for electrode and electrolytes during an electrochemical process is a crucial issue to further improve the performance of lithium ion batteries (LIB). In this study, we systematically investigate the interaction between propylene carbonate (PC)-based electrolytes and graphite anode material, which has been under dispute for a long time in the electrochemical community, and a new physical model is proposed to explain the poor compatibility of PC with graphite. With the aid of scanning electron microscopy, focused ion beam workstation, Raman spectroscopy, X-ray photoelectron spectroscopy, X-ray diffraction, and thermogravimetry−differential scanning calorimetry, the cumbersome but intriguing questions on the poor compatibility are addressed: (i) Does PC truly have the ability to co-intercalate into graphite materials? Our answer is yes. (ii) Where is the intercalation site? It is around the crystal boundary. (iii) Why does the co-intercalation occur for PC not ethylene carbonate—another kind of useful electrolyte in LIB, since both of them have a similar molecular structure? The methyl group in the PC molecule is the main wire-puller, which makes decomposition products of PC puffed and thus incompetent in inhibiting the subsequent co-intercalation. Finally, three feasible strategies to overcome the poor compatibility are summarized.

Introduction

Nowadays, lithium ion batteries (LIB) are powering most portable electronic products, and its potential application in hybrid electric vehicles (HEVs) or electric vehicles (EVs) has been attracting extensive interest all over the world this past decade.[1−6] To achieve the goal of high energy and power density for LIB, a systematic experimental and theoretical work is needed: on one hand, studies on excellent electrode materials, stable electrolytes, proper separators, and other auxiliary components are pivotal; on the other hand, a deep understanding of related electrochemical phenomena and processes accompanying electrode reactions is also definitely imperative. It is well known among the electrochemical community that the interaction (or compatibility) between electrode materials and electrolytes is an important issue, which to a great extent determines the performance of the properties of LIB such as the first Coulombic efficiency, cycle life, power capability, and safety, etc.[7−8]

Currently, the most suitable solvents for liquid rechargeable LIB remain the mixtures of cyclic and linear alkyl carbonates such as propylene and ethylene carbonates (PC, EC) and dimethyl and diethyl carbonates (DMC, DEC), respectively.[8] Both PC and EC demonstrate a wide electrochemical stability window, high ionic conductivity,[9] and a similar cyclic molecular structure as shown in Figure 1, but there is a remarkable difference in the melting point for them: the former is approximately −49 °C, the latter approximately 39 °C.[10] Obviously, the low-melting-point PC makes it easy to enlarge the application field of LIB, especially for the situation at a relatively low-working temperature. Unfortunately, the compatibility of PC with the graphite anode widely used in current

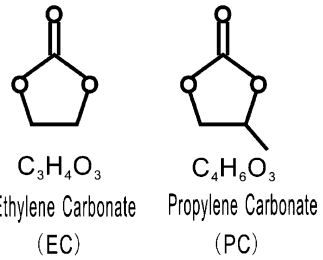

Figure 1. Schematic drawing of the molecular structure of EC and PC.

LIB is very poor.[11−15] In most cases, no reversible capacity can be delivered. Many researchers have attempted to investigate the reasons for this problem, because clarifying the interactions will make it helpful to understand the surface chemistry of electrode materials, to design optimum electrolyte solutions, and finally to develop high-performance LIB. Until now, two different physical models are documented to explain the destructive behavior of PC. Besenhard et al.[16−17] considered that solvent molecules (e.g., PC) could co-intercalate into graphite to form a ternary graphite intercalation compound $[Li_x(solv)_yC_n]$, and its decomposition products among graphene layers caused graphite exfoliation. Nevertheless, Peled et al.[18] emphasized the inability of PC-based electrolytes to form a stable solid electrolyte interphase (SEI) film on the surface of graphite. Aurbach et al.[19−22] further attributed the failure of PC to its continuous reduction and decomposition accompanied by the production of gases (e.g., C_3H_6), and the decomposition products disconnect graphite particles from bulk electrode, finally leading to graphite deactivation because of electrical isolation. In brief, the first mechanism is a three-dimensional reaction process (i.e., co-intercalation), and the second is a surface reaction (i.e., reduction and decomposition). So far, each model can gain some support from a few experimental observa-

* Corresponding author. E-mail: cheng@imr.ac.cn. Fax: +86 24 2390 3126.

10.1021/jp066762j CCC: $37.00
Published on Web 03/08/2007

tions. For example, the evidence of topographical changes on highly ordered pyrolytic graphite (HOPG) noted by Inaba and Ogumi et al. using scanning tunneling microscopy (STM)[23−24] and atomic force microscopy (AFM),[25−26] and of macroscopic expansion from in situ electrochemical dilatometry reported by Winter et al.,[27] mainly favors the phenomenon of co-intercalation, yet the results according to Fourier transform infrared spectroscopy (FTIR), X-ray photoelectron spectroscopy (XPS), and X-ray diffraction (XRD)[28−29] are in support of the viewpoint of surface reaction. Despite considerable effort, there are still uncertainties for each scenario: the phenomenon of co-intercalation into graphene layers lacks the approval from XRD and clearer images (e.g., SEM) to indicate the expansion of interlayer spacing; the viewpoint of surface reaction cannot explain why certain graphite materials (e.g., with a high amount of rhombohedral phase) are compatible with PC-based electrolytes.[30−31]

How to deal with the contradiction in the two scientific scenarios has been an open question, which is partially ascribed to the complexity of interfacial chemistry between electrode materials and electrolytes. Possibly, the two kinds of interfacial processes (co-intercalation and surface decomposition reaction) exist simultaneously/competitively on the surface of graphite. Or, the co-intercalation occurs, but the intercalation site is not at all within interlayers. In addition, most of the previous studies (STM, AFM, XPS, FTIR, etc.) only focus on the surface changes of graphite particles. There are no reports on what really happens to the internal texture of graphite because of the limitation in characterization instruments. Therefore, it is hard to make a convincing conclusion that PC indeed co-intercalates into the graphite host.

In a previous work,[32] we first employed a focused-ion-beam (FIB) technique to investigate the formation and evolution of the SEI film on the surface and inside of natural graphite spheres, since the FIB technique has an ability to accurately cut a specimen (in the scale of micrometers or nanometers) at any user-defined position, thus providing an opportunity to obtain a cross section for studying internal microstructure. Here we again utilize the FIB technique and incorporate other spectroscopic, morphological, structural, and thermal analyses such as XPS, Raman spectroscopy, scanning electron microscopy (SEM), XRD, and thermogravimetry−differential scanning calorimetry (TG−DSC) to systematically examine the interactions between PC-based electrolytes and graphitized mesocarbon microbeads (MCMB). Meanwhile, on the basis of as-obtained experimental results, we also combine theoretical considerations to gain a deeper understanding of the interaction features. In a word, the following cumbersome but intriguing questions are addressed with the aid of both experimental and theoretical fruits in this study: (1) Does PC truly have the ability to co-intercalate into graphite? (2) If so, where are the intercalation sites? Graphene interlayers or others? (3) Why does the poor compatibility belong to PC not EC, since both of them have a similar molecular structure except for the additional methyl group in PC?

Experimental Section

Because highly graphitized MCMB (heat treatment at 2800 °C, Osaka Gas Co., Ltd.) with very similar crystalline structure to graphite is extensively used as anode material in commercial LIB, we chose it as electrode active material to investigate its interactions with PC-based electrolytes, which ensures our study will be representative.

For electrochemical measurements, half-cells were assembled in an Ar-filled glovebox (Mbraun, Unilab, H_2O and O_2 < 1 ppm) with a working electrode, a lithium foil counter electrode, and a porous separator (Celgard 2400). The detailed processes on electrode preparation can be found in refs 33−34. The PC-based and EC-based electrolytes (battery grade, from Shanshan Tech Group, China) are respectively as follows: 1 M $LiPF_6$ in a mixture of PC and DMC (1:2 by volume), and 1 M $LiPF_6$ in EC/DMC (1:1 by volume).

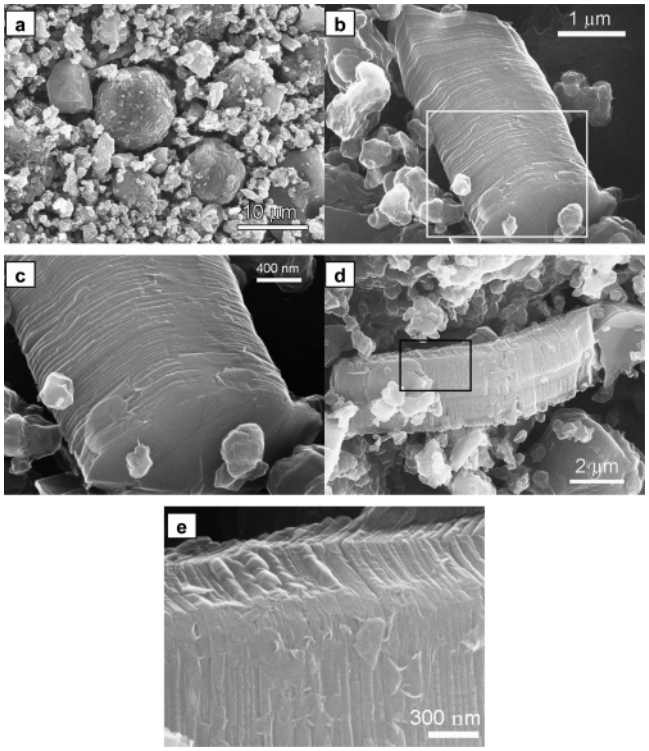

Figure 2. SEM images of the original MCMB: (a) spherical particles with various sizes; (b and d) the columned- and prism-shaped objects, respectively; (c and e) the corresponding magnified images of the rectangles in panels b and d.

The cells were galvanostatically discharged/charged (corresponding to lithiation and delithiation process, respectively) at a current density of 0.2 mA/cm^2 between 0.001 and 2.5 V versus Li^+/Li. After reaching preset electrochemical states in PC or EC-based electrolytes, the cells were dismantled in the glovebox, and the working electrode was taken out and washed using DMC solution. Subsequently, it was heated in vacuum at 60 °C to remove the residual DMC and then transferred using a sealed container into the vacuum chamber of FIB (Nova 200, Nanolab), SEM (LEO-Supra35), and XPS (Escalab 250, Al kα) apparatus for corresponding characterization. To avoid the exposure in air during XRD measurement (D/max 2400 with Cu kα radiation), the cycled working electrode was coated by a layer of vacuum grease, which is not reactive with the electrode surface. To collect Raman spectra (Labram HR 800, Jobin-Yvon), an airtight sample pool was specifically designed with a quartz glass window allowing laser to pass. For TG−DSC testing (Netzsch-STA 449C), the active material was first scraped from the cycled working electrode and then quickly transferred into the heating furnace with flowing Ar as protection. The subsequent heating was performed from room temperature to 350 °C at a rate of 5 °C/min and under an Ar flow rate of 10 mL/min.

Results and Discussion

Figure 2a displays SEM images of the original MCMB powders, where most of the spherical particles, whose crystallite

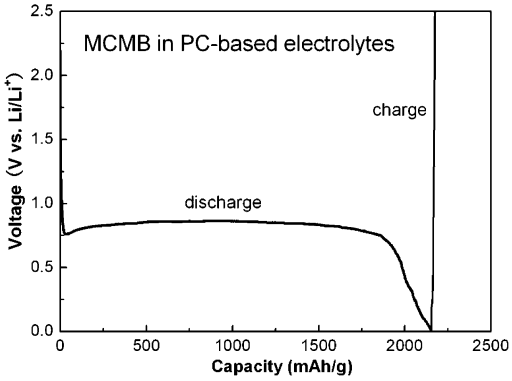

Figure 3. A typical voltage profile for the MCMB in PC-based electrolytes.

orientation has a radial-like texture,[35] are in the size range from several to tens of micrometers. The combination of particles with various sizes is beneficial to the stacking density of electroactive materials, thus improving the volumetric energy density of LIB. In addition, some columned- and prismshaped objects are also noted in the MCMB sample (see Figure 2b and d). Usually, they are concomitants during the extraction of pitch to isolate mesophase spherules.[36] From the magnified images in Figure 2c and e, it can be seen that their crystallites stack approximately parallel to each other (as demonstrated by Figure S1 in Supporting Information). The MCMB sample displays excellent electrochemical performance in EC-based electrolytes, and its voltage profile and cycling performance are available in Supporting Information.

Figure 3 demonstrates the voltage profile of MCMB in PC-based electrolytes for the first discharge/charge process. It can be noted that there are no voltage plateaus below 0.2 V corresponding to the reversible intercalation of Li ions, but a long discharge plateau at ~0.8 V generally attributed to the decomposition or co-intercalation of PC[9,17,37] is observed. Meanwhile, in the subsequent charge process, the voltage promptly jumps to the cutoff (2.5 V) without any capacity delivered. To investigate what happens to the MCMB in the PC-based electrolytes, a cell after experiencing the first discharge was dismantled, and its electroactive material was subject to the following characterizations.

Figure 4 panels a−f exhibit the morphological changes of the columned- and prismshaped objects after the first discharge through secondary electron FIB images, where a series of intriguing accordion-like shapes clearly indicate that PC can co-intercalate into graphite, because only the surface decomposition reaction of PC never causes those expansion features (particularly see Figure 4c−d). After PC co-intercalation, each expansion unit is separated by the solvated Li^+ ($Li_x(solv)_y$). To exclude the possibility that the unique expansion feature is due to the effect of macropenetration of electrolytes and/or of single Li^+ intercalation, we also examined the situation of MCMB in the EC-based electrolytes, and found that even after 10 electrochemical cycles the columned- and prism-shaped objects still remain in their original shapes without expansion. A detectable change is that their surface becomes relatively smooth because of the coating of a compact SEI film (see Supporting Information). Therefore, it can be convincingly concluded that PC truly has the ability of co-intercalation. It needs to be pointed out that the direct and evident images we obtained here is significantly attributed to the existence of those columned- and prism-shaped objects, which have an appropriate crystallite orientation (see Figure S1 in Supporting Information) and thus provide a great opportunity for PC to approach and subsequently cause the expansion.

By carefully observing Figure 4b−f, we note that the intercalation sites of PC are not random but regular, and the thickness of each expansion unit is similar. Figure 4 g presents the statistic distribution of the thickness for those expansion units in Figure 4b, and the mean value is ~150 nm which is comparable to the scale of a crystallite. It is well known that in a polycrystalline material the crystal boundary is not stable with high energy. Consequently, it is possible that each expansion unit shown here is just a crystallite, and the intercalation site is located on the crystal boundary. If it is true that PC cannot co-intercalate into the graphene interlayers within a crystallite, decomposition reaction of electrolytes will occur unavoidably on the surface of the crystallite. Then, the relative content of fluorine (F), oxygen (O), carbon (C), and phosphorus (P), which are the main elements constituting the decomposition products of electrolytes,[32] should be higher on the surface of each crystallite than around the crystal boundary. To verify this point, we performed the elemental line scan analysis (ELSA) along the white line in Figure 4f, and the results are shown in Figure 4h. It can be seen that the ELSA curve of each element shows alternate peaks and valleys, which exactly correspond to a crystallite and a neighbored crystal boundary, respectively.

So far, based on the experimental facts mentioned above, we can propose a new model for the destructive behavior of PC as shown in Figure 5. In a crystallite of polycrystalline graphite, all graphene layers have the same angular orientation, but the orientation is different from that in an adjacent crystallite. As a result, there is an opening around the crystal boundary, which is more easily accessible to solvated Li^+ (e.g., $Li_x(PC)_y$) compared to the normal interlayer spacing. The co-intercalation of solvated Li^+ further enlarges the boundary spacing, and finally leads to macrocracking and separation (as actually shown in Figure 4a−f).

Frankly, the evidence for the co-intercalation of PC and its intercalation site is a little presentational in the former discussion, mainly in terms of morphological changes. To further confirm our model, a micro-Raman spectrometer (~1 μm^2 spot area, HeNe laser 632.8 nm) was employed to probe the structural information. Figure 6 exhibits the comparison of Raman spectra including the typical D-, G-, D′-, and G′-band among the original MCMB, the MCMB experiencing 10 electrochemical cycles in EC-based electrolytes, and the MCMB after the first discharge in PC-based electrolytes. It can be noted in Figure 6a that the intensity of the D-band is remarkably increased relative to the one of the G-band for the sample in PC-based electrolytes. But the case of EC-based electrolytes is different, with a weak D-band which is nearly the same as that for the original MCMB. Meanwhile, the D′-band (see the dotted lines by peak fitting) for the three samples also demonstrates the similar variation characteristics as the D-band. In fact, the Raman bands (i.e., D-, G-, D′-, and G′-band) for the MCMB (finally at delithiation state) in EC-based electrolytes are totally similar to those for the original one (see Figure 6a−b), which implies that the intercalation/de-intercalation of a single Li^+ into the graphite host is a highly reversible process almost without any structural deterioration. However, the significantly changed Raman spectrum in PC-based electrolytes indicates the occurrence of certain structural alternation. It is well-known that the D- and D′-band are activated in the second-order scattering process, mostly relating to the structural disorder and defect (e.g., crystal boundary) that lower the crystalline symmetry of the quasi-infinite lattice of graphite.[38] Therefore, an increased intensity

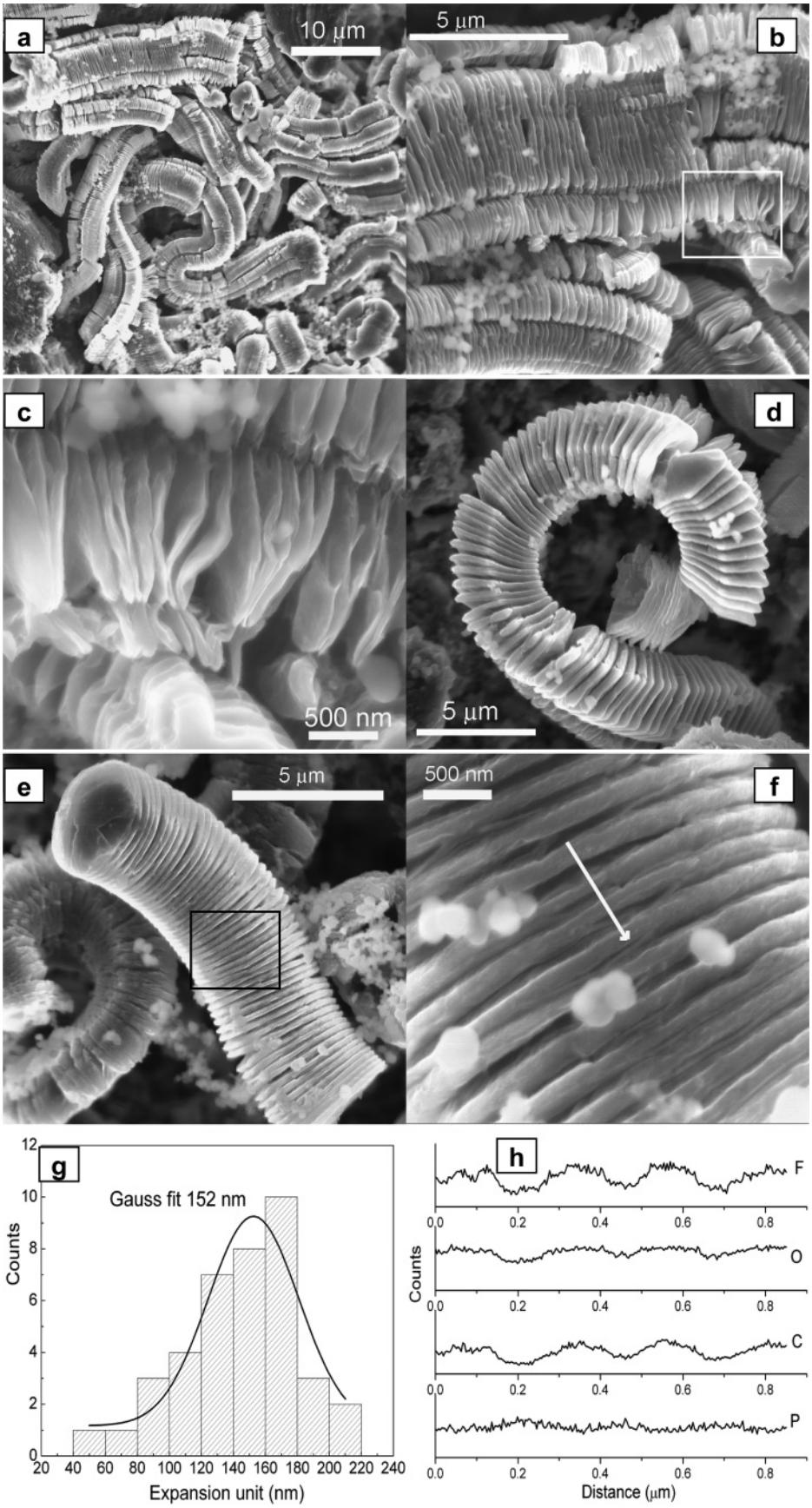

Figure 4. (a−f) The FIB secondary electron images of the columned- and prism-shaped objects after experiencing the first discharge in PC-based electrolytes. Panels c and f show the magnified images of the rectangles in panels b and e, respectively; (g) the statistic distribution of the thickness of those expansion units in panel b; (h) the ELSA analysis along the white line in panel f.

in D-band indicates the presence of a large amount of defects in the graphite matrix. According to the Daumas and Hérold (DH) model of intercalation compounds,[39] the existence of an intercalant may cause the defects. Here, the intercalant should

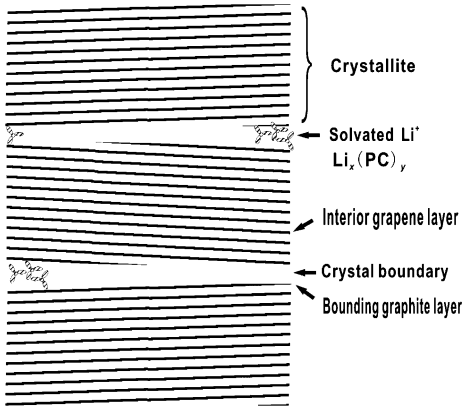

Figure 5. Schematic drawing of our new model for the mechanisms of co-intercalation of PC.

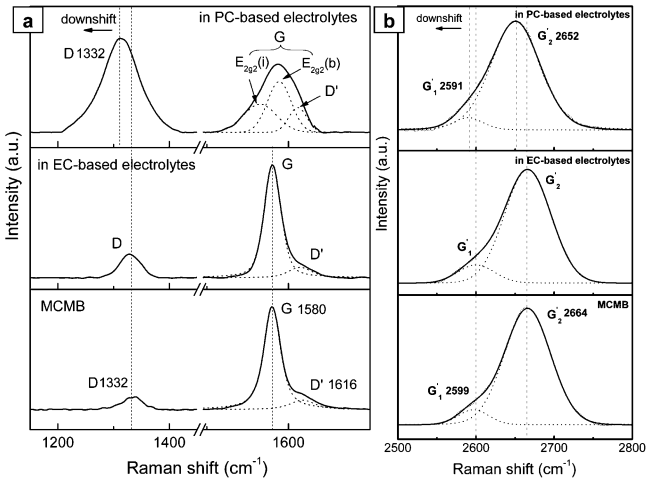

Figure 6. Comparison of Raman spectra among the original MCMB, the MCMB after 10 cycles in EC-based electrolytes (finally at delithiation state), and the MCMB experiencing the first discharge in PC-based electrolytes: (a) D-, G-, and D′-band; (b) G′-band.

be the solvated Li^+ (i.e., $Li_x(PC)_y$). However, it is obvious that only according to the changes of D-band we cannot get sufficient support for the co-intercalation of PC. Fortunately, G-band, the first-order Raman peak due to in-plane E_{2g} optical phonon mode, can bring us powerful knowledge: when an intercalation reaction occurs, a doublet structure at frequencies close to the pristine singlet G-band peak will be found.[40−42] This is because there are two different vibration environments for carbon atoms as demonstrated in Figure 5: one is the bounding graphite layer where the lattice mode is denoted by E_{2g2}(b); the other is the interior graphite layer with a mode of E_{2g2}(i). In our experiment, the doublet structure of G-band was indeed observed for the MCMB in PC-based electrolytes (see Figure 6a). Hence, the first question proposed in the Introduction section can be convincingly answered now: PC does co-intercalate into graphite. To solve the question about the intercalation site, we investigated the second-order G′-band that is symmetry-allowed and is an intrinsic property of all sp^2 carbons, generally exhibiting a doublet structure due to good interlayer coupling (i.e., ABAB stacking).[43−44] But when the stacking order is disturbed such as transforming into AA coupling, the doublet peak will coalesce to a single one.[45] Consequently, the G′-band can be a fingerprint to indicate the stacking changes. It was reported that Li^+ intercalation into graphene layers is able to reversibly shift the AB layer to the AA layer stacking to lower the overall energy of the system.[46−47] If the co-intercalation of solvated Li^+ is also between graphene interlayers, the transformation should occur in the same way, and then a single G′-band will be detected. Nevertheless, the situation is just opposite in Figure 6b. A doublet structure (G_1' and G_2') is demonstrated for the MCMB in PC-based electrolytes, which indicates that the intercalation site can only be around the crystal boundary as shown in Figure 5.

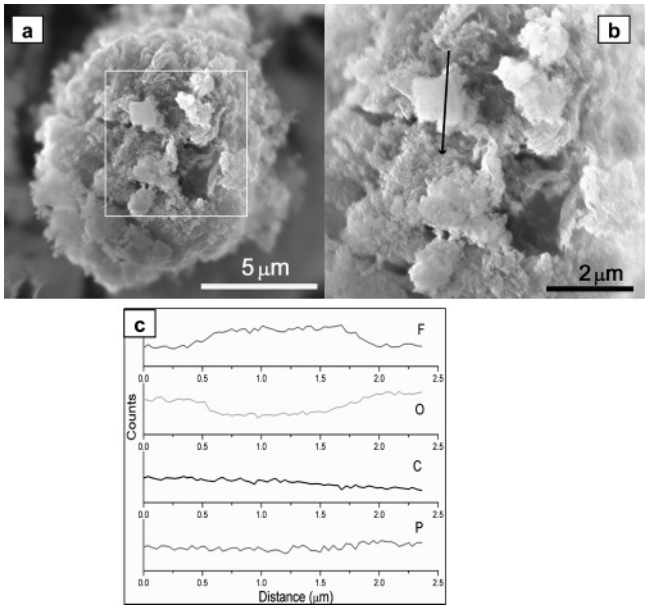

Figure 7. (a) FIB secondary electron image for an MCMB spherule experiencing the first discharge in PC-based electrolytes; (b) the magnified image of the rectangle in panel a; (c) the ELSA analysis along the black line in panel b.

Since the spherical particles are the main components in the original MCMB sample, we should pay more attention to them in our investigation. Figure 7 displays FIB secondary electron images and corresponding ELSA curves for the spherules after they experienced the first discharge in PC-based electrolytes. It can be seen in Figure 7a−b that their surface becomes puffed with some bulk particles randomly distributed. For comparison, the image of an MCMB sphere after 10 electrochemical cycles in EC-based electrolytes is displayed in Supporting Information, where the surface is coated by a layer of compact and relatively smooth SEI film, totally different from what is shown here. Figure 7c shows the ELSA analysis along the black line in Figure 7b: there are no obvious changes for C and P, but the content of F increases and O decreases when the scan line passes through that bulk particle. This variation feature implies that the puffed surface is mostly made up of decomposition products of solvents (e.g., $ROCO_2Li$, ROLi, etc.), and those bulk particles are inorganic reduction products of salt anion (e.g., LiF).

To confirm this point, XPS was employed to investigate the surface and depth composition. Figure 8 displays the spectra of C 1s, F 1s, and O 1s under a series of Ar ion-beam sputtering time (0 s, 30, 150, and 450 s) for the sample in PC-based electrolytes. Out of consideration for clarity, all spectra are displayed without any peak fitting, but the typical peak positions of various decomposition products are marked on the basis of refs 48−54. In Figure 8a, it can be seen that the C 1s spectra contain the contributions from hydrocarbons (C−H), polymers (C−O−C), Li−alkyl carbonates ($ROCO_2Li$), and Li_2CO_3, etc. in the whole sputtering process, indicating that electrolytes decompose continuously with the formation of a thick SEI film. The F 1s spectra (Figure 8b) show that $LiFP_6$ (the existence of $LiFP_6$ is also proved by the P 2p spectra, not shown here) and LiF are mainly responsible for the F-containing species on the

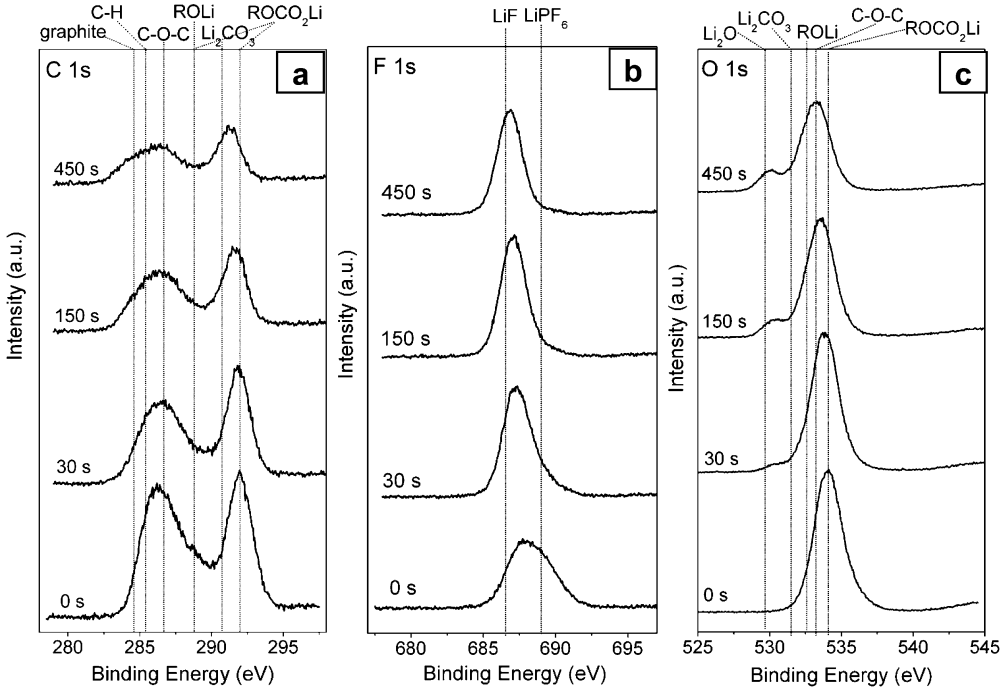

Figure 8. XPS data at different sputtering time from 0 to 450 s, showing the C 1s, F 1s, and O 1s spectra for the MCMB after the first discharge in PC-based electrolytes.

surface before sputtering (0 s). With the increase in sputtering depth, LiF progressively becomes the majority, which means that the salt decomposes mostly in the beginning of the formation of SEI film.[54] Figure 8c exhibits the O 1s spectra, where the main peak is from $ROCO_2Li$, ROLi, and C−O−C. This result is in agreement with that analyzed in C 1s spectra. A weak peak at ~528.7 eV appears after sputtering of 150 s, which is assigned to Li_2O owing to the sputter-induced decomposition of Li−alkyl carbonates.[14] Altogether, the XPS data indicate that PC-based electrolytes decompose violently on the electrode surface accompanying a large amount of Li−alkyl carbonates. However, the XPS results of the MCMB in EC-based electrolytes (see Supporting Information) reveal different decomposition products and few Li−alkyl carbonates constituting the SEI film. Finally, it needs to be pointed out that in the C 1s and F 1s spectra there is some participation of PVDF binders. But their contribution is limited and does not influence our above discussion.

Quantitatively, if it is true that the amount of Li−alkyl carbonates is more in the case of PC-based electrolytes than in EC-based electrolytes, there will be a larger weight loss for the former than the latter when the cycled MCMB is heated. This is because Li−alkyl carbonates can decompose with the release of CO_2 in a heating process.[55−57] We performed the TG−DSC analysis (see Supporting Information) for the MCMB samples after cycling in both electrolytes, and the weight loss is 19.9% for the former and 1.6% for the latter. The results sufficiently confirm that there is a large amount of decomposition products for the MCMB in PC-based electrolytes. Therefore, the down-shift of D- and G′-band (see the Raman spectra in Figure 6) can now be explained: on one hand, the two bands have a strongly dispersive behavior—their frequencies are significantly dependent on the laser excitation energy;[44] on the other hand, the big accumulation of decomposition products on the surface influences the absorption of incident laser.

Figure 9 demonstrates the comparison of XRD patterns. For the sample after 10 cycles (finally at the delithiation state) in EC-based electrolytes, there is nearly the same pattern as with

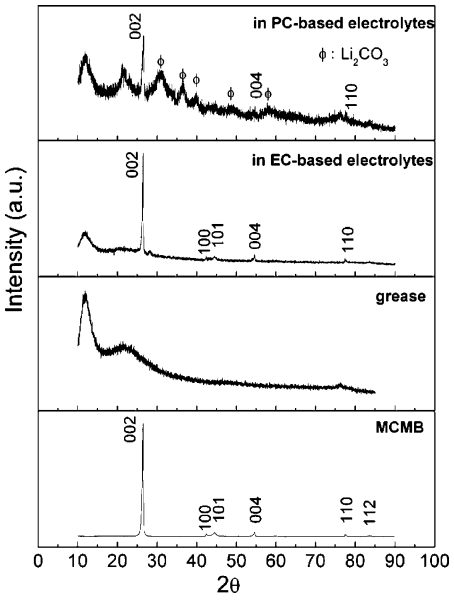

Figure 9. XRD patterns for the original MCMB, the vacuum grease, the MCMB experiencing 10 cycles in EC-based electrolytes, and the MCMB after the first discharge in PC-based electrolytes.

the original one, except for the peak at ~11.5° attributed to the vacuum grease, which means that single Li^+ intercalation is a highly reversible process without obviously changing the crystalline structure of graphite. This result is in good agreement with that from Raman spectra (see Figure 6). However, for the sample experiencing the first discharge in PC-based electrolytes, an evident variation can be noted in the pattern: there are peaks from Li_2CO_3, and the 002 graphite diffraction peak remains at its original position but becomes relatively weak in comparison with the main peak (at ~11.5°) of vacuum grease. All of these phenomena confirm once more that there is indeed a large amount of decomposition products in PC-based electrolytes, and PC does not co-intercalate into graphene layers (if so, the 002

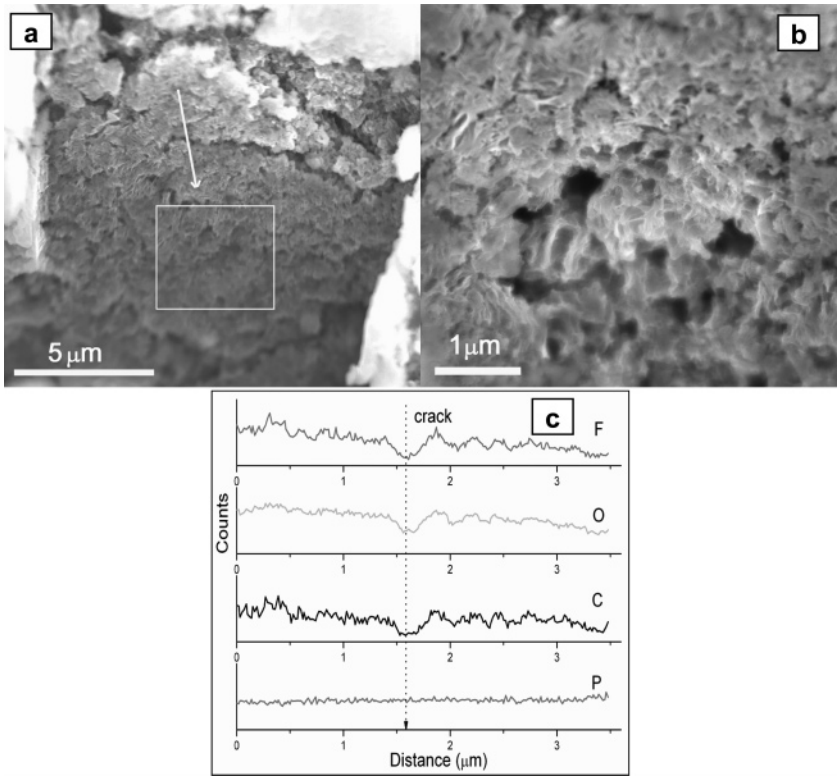

Figure 10. (a) FIB secondary electron image showing the cross section of an MCMB spherule experiencing the first discharge in PC-based electrolytes; (b) the magnified image of the rectangle in panel a; (c) ELSA analysis along the white line in panel a.

peak will shift downward). but into the crystal boundary to weaken the crystalline degree (i.e., the lowering of 002 peak intensity).

According to the above discussion on the MCMB spherules, we can conclude undoubtedly that PC-based electrolytes decompose violently on the electrode surface and the products are not dense and compact. But we do not yet observe the apparently morphological proof of co-intercalation of PC into the spherules, which is mainly due to different crystallite stacking orientations in the spherules. To tackle this problem, we utilized a FIB workstation to cut a spherule and then investigated its internal texture. Figure 10panels a−b show FIB secondary electron images for the cross-section of the spherule. To the best of our knowledge, this is the first time there was a direct probe of the interior of electroactive materials after cycling in PC-based electrolytes. It can be easily seen that there are many cracks and holes inside the spherule, which are not observed in the original cross-section of the uncycled MCMB sample. Clearly, the exclusive surface decomposition of electrolytes is not enough to cause these defects. As proposed in our model (see Figure 5), the co-intercalation of PC into crystal boundary should be responsible for the unique phenomenon. Furthermore, Figure 10c shows the ELSA analysis along the white line in Figure 10a, where the elements of F, O, C, and P are all detected. Therefore, the whole destructive process of PC-based electrolytes can be summarized as follows: first, the electrolytes decompose on the electrode surface, but the products are puffed and cannot inhibit the co-intercalation of PC; second, the co-intercalation of PC into the crystal boundary causes the splitting of electroactive materials (the splitting is commonly named "intergranular fracture" in a polycrystalline material[58]) and the formation of a fresh inner surface; third, the electrolytes penetrate into those cracks and holes and decompose on the newly exposed surface (the process is responsible for the existence of F, O, C, and P inside the MCMB sphere); fourth, the co-intercalation occurs again accompanying the decomposition reaction. In a word, this —"chain reaction"— is carried out repeatedly and finally leads to the destruction of the electrode and the consumption of electrolytes.

Now, the third question in the Introduction has been partly answered: the decomposition products of PC are not compact enough, which allows the occurrence of co-intercalation. Then, why are they puffed for PC-based electrolytes not for EC-based electrolytes? The answer is relatively complex, but fortunately theorists have performed some theoretical computations.[7,59−62] It is speculated that the decomposition products from PC twist more considerably than that from EC because of the steric hindrance of the extra methyl group, which blocks the 3-D dense growth of SEI film.[7,62] Our experimental observations completely prove this speculation. As to why the intercalation site is preferably around the crystal boundary rather than graphene interlayers, computations by Wang et al.[62] also give some clues: the trimer of PC with Li^+ can exert a significant deformation on the graphite surface. Hence, on the basis of our knowledge of molecular-strain energy obtained in polycyclic aromatic hydrocarbons,[63] considerable nonplanar-strain energies may be induced when PC co-intercalates into the graphene interlayers except for getting over the ply adhesion. However, the nonplanar-strain energy can be partly released through bay areas[63] around the crystal boundary, and the sizable spacing of crystal boundary is also favorable for the accommodation of solvated Li^+. In conclusion, our new model (see Figure 5) on the co-intercalation of PC is not in conflict with all experimental phenomena reported previously and observed here and is reasonable from the theoretical standpoint, too.

Finally, it needs to be pointed out that there are two preconditions on the side of graphite for the occurrence of PC co-intercalation: first, a proper entry must be provided by the graphite host; second, the size of the crystallite should be big enough to screen the interference from an adjacent intercalant.

If the two conditions cannot be satisfied, PC will only decompose on the surface and no chain reaction will be triggered. When the decomposition products accumulate to some extent, a reversible intercalation of Li^+ may take place. Our preliminary investigation on the electrochemical performance of graphitized and nongraphitized multiwall carbon nanotubes and disordered pyrolytic carbon in PC-based electrolytes has proved this point. Therefore, there are three feasible strategies to overcome the poor compatibility of PC with graphite: (i) modifying the surface structure of graphite to restrict the entrance for PC, for example, coating a layer of disordered carbon; (ii) designing a new type of electrolytes and considering the effect of a methyl group in the molecular structure at the very beginning; (iii) building a dense SEI film beforehand on the electrode surface by some electrolyte additives such as vinylene carbonate,[64] ethylene sulfite,[65] SO_2,[66] etc. or by precycling the electrode in some stable electrolytes.

Conclusions

On the basis of the above systematic discussion, we propose a new model about the interactions between PC-based electrolytes and graphite anode material and conclude the following definite viewpoints: (i) PC does have the ability of co-intercalation; (ii) the intercalation site is around the crystal boundary; (iii) the existence of a methyl group makes decomposition products of PC puffed, which cannot inhibit the subsequent co-intercalation but will cause a chain reaction.

The meaningful fruits obtained here, we believe, not only deepen the understanding and knowledge of the surface chemistry of electrode and electrolytes, but also are helpful and revelatory for the design of electrolyte systems, the modification of electroactive materials, and finally the practical development and manufacture of high performance LIB.

Acknowledgment. The authors thank Dr. W. C. Ren for helpful discussions on Raman spectroscopy. The work was supported by National Natural Science Foundation of China (No. 90606008, 50632040, and 50472084) and MOST of China (No. 2006CB932703).

Supporting Information Available: Schematic drawing of the stacking direction for the crystallites of columned- and prism-shaped objects in MCMB; voltage profile, cycling performance, SEM images, and XPS data for the MCMB in EC-based electrolytes; TG−DSC curve. This material is available free of charge via the Internet at http://pubs.acs.org.

References and Notes

(1) Kang, K.; Meng, Y. S.; Bréger, J.; Grey, C. P.; Ceder, G. *Science* **2006**, *311*, 977−980.

(2) Taberna, P. L.; Mitra, S.; Poizot, P.; Simon, P.; Tarascon, J. M. *Nat. Mater.* **2006**, *5*, 567−573.

(3) Linden D.; Reddy T. B. *Handbook of Batteries*; McGraw-Hill: New York, 2002; pp 35.1−35.9.

(4) Tarascon, J. M.; Armand, M. *Nature* **2001**, *414*, 359−367.

(5) Vetter, J.; Novák, P.; Wagner, M. R.; Veit, C.; Möller, K. C.; Besenhard, J. O.; Winter, M.; Wohlfahrt-Mehrens, M.; Vogler, C.; Hammouche, A. *J. Power Sources* **2005**, *147*, 260−281.

(6) Tirado, J. L. *Mater. Sci. Eng., R* **2003**, *40*, 103−136.

(7) Balbuena, P. B., Wang, Y. X., Eds. *Lithium-Ion Batteries Solid-Electrolyte Interphase*; Imperial College Press: London, 2004; pp xiii−xv; 227−275.

(8) Aurbach, D. In *Advances in Lithium-Ion Batteries*; Schalkwijk, W. A., Scrosati, B., Eds.; Kluwer: New York, 2002; pp 7−77.

(9) Chung, G. C.; Kim, H. J.; Yu, S.; Jun, S. H.; Choi, J. W.; Kim, M. H. *J. Electrochem. Soc.* **2000**, *147*, 4391−4398.

(10) Wakihara, M. *Mater. Sci. Eng. R* **2001**, *33*, 109−134.

(11) Kaneko, H.; Sekine, K.; Takamura, T. *J. Power Sources* **1995**, *146*, 142−145.

(12) Fujimoto, M.; Shoji, Y.; Kida, Y.; Ohshita, R.; Nohma, T.; Nishio, K. *J. Power Sources* **1998**, *72*, 226−230.

(13) Ein-Eli, Y. *Electrochem. Solid-State Lett.* **1999**, *2*, 212−214.

(14) Herstedt, M.; Andersson, A. M.; Rehsmo, H.; Siegbahn, H.; Edström, K. *Electrochim. Acta* **2004**, *49*, 4939−4947.

(15) Buqa, H.; Würsig, A.; Goers, D.; Hardwick, L. J.; Holzapfel, M.; Novák, P.; Krumeich, F.; Spahr, M. E. *J. Power Sources* **2005**, *146*, 136−141.

(16) Besenhard, J. O.; Winter, M.; Yang, J.; Biberacher, W. *J. Power Sources* **1995**, *54*, 228−231.

(17) Winter, M.; Besenhard, J. O.; Spahr, M. E.; Novák, P. *Adv. Mater.* **1998**, *10*, 725−763.

(18) Peled, E.; Golodnitsky, D.; Penciner, J. In *Handbook of Battery Materials*; Besenhard, J. O. Ed.; Wiley-VCH: Weinheim, Germany, 1999; pp 419−456.

(19) Aurbach, D.; Levi, M. D.; Levi, E.; Schechter, A. *J. Phys. Chem. B* **1997**, *101*, 2195−2206.

(20) Aurbach, D.; Koltypin, M.; Teller, H. *Langmuir* **2002**, *18*, 9000−9009.

(21) Aurbach, D. *J. Power Sources* **2000**, *89*, 206−218.

(22) Aurbach, D. *J. Power Sources* **2003**, *119*−*121*, 497−503.

(23) Inaba, M.; Siroma, Z.; Kawatate, Y.; Funabiki, A.; Ogumi, Z. *J. Power Sources* **1997**, *68*, 221−226.

(24) Inaba, M.; Kawatate, Y.; Funabiki, A.; Jeong, S. K.; Abe, T.; Ogumi, Z. *Electrochim. Acta* **1999**, *45*, 99−105.

(25) Jeong, S. K.; Inaba, M.; Abe, T.; Ogumi, Z. *J. Electrochem. Soc.* **2001**, *148*, A989−A993.

(26) Jeong, S. K.; Inaba, M.; Iriyama, Y.; Abe, T.; Ogumi, Z. *Electrochim. Acta* **2002**, *47*, 1975−1982.

(27) Winter, M.; Wrodnigg, G. H.; Besenhard, J. O.; Biberacher, W.; Novák, P. *J. Electrochem. Soc.* **2000**, *147*, 2427−2431.

(28) Aurbach, D.; Markovsky, B.; Weissman, I.; Levi, E.; Ein-Eli, Y. *Electrochim. Acta* **1999**, *45*, 67−86.

(29) Jiang, Z.; Alamgir, M.; Abraham, K. M. *J. Electrochem. Soc.* **1995**, *142*, 333−340.

(30) Guerin, K.; Fevrier-Bouvier, A.; Flandrois, S.; Couzi, M.; Simon, B.; Biensan, P. *J. Electrochem. Soc.* **1999**, *146*, 3660−3665.

(31) Herstedt, M.; Fransson, L.; Edström, K. *J. Power Sources* **2003**, *124*, 191−196.

(32) Zhang, H. L.; Li, F.; Liu, C.; Tan, J.; Cheng, H. M. *J. Phys. Chem. B* **2005**, *47*, 22205−22211.

(33) Zhang, H. L.; Zhang, Y.; Zhang, X. G.; Li, F.; Liu, C.; Tan, J.; Cheng, H. M. *Carbon* **2006**, *44*, 2778−2784.

(34) Zhang, H. L.; Liu, S. H.; Li, F.; Bai, S.; Liu, C.; Tan, J.; Cheng, H. M. *Carbon* **2006**, *44*, 2212−2218.

(35) Tatsumi, K.; Iwashita, N.; Sakaebe, H.; Shioyama, H.; Higuchi, S. *J. Electrochem. Soc.* **1995**, *142*, 716−720.

(36) Chang, Y. C.; Sohn, H. J.; Ku, C. H.; Wang, Y. G.; Korai, Y.; Mochida, I. *Carbon* **1999**, *37*, 1285−1297.

(37) Zhang, S. S.; Xu, K.; Jow, T. R. *J. Power Sources* **2006**, *156*, 629−633.

(38) Dresselhaus, M. S.; Dresselhaus, G.; Saito, R.; Jorio, *Phys. Rep.* **2005**, *409*, 47−99.

(39) Clarke, R.; Uher, C. *Adv. Phys.* **1984**, *33*, 469−566.

(40) Huang, W. W.; Frech, R. *J. Electrochem. Soc.* **1998**, *145*, 765−770.

(41) Hardwick, L. J.; Buqa, H.; Novák, P. *Solid State Ionics* **2006**, *26*−*32*, 2801−2806.

(42) Dresselhaus, M. S.; Dresselhaus, G. *Adv. Phys.* **2002**, *51*, 1−186.

(43) Mennelia, V.; Monaco, G.; Colangeli, L.; Bussoletti, E. *Carbon* **1995**, *33*, 115−121.

(44) Dresselhaus, M. S.; Eklund, P. C. *Adv. Phys.* **2000**, *49*, 705−814.

(45) Wilhelm, H.; Lelaurain, M.; McRae, E. Humbert, B. *J. Appl. Phys.* **1998**, *84*, 6552−6558.

(46) Guerard, D.; Herold, A. *Carbon* **1975**, *13*, 337−345.

(47) Shi, H.; Barker, J.; Saidi, M. Y.; Koksbang, R. *J. Electrochem. Soc.* **1996**, *143*, 3466−3472.

(48) Kanamura, K.; Tamura, H.; Shiraishi, S.; Takehara, Z. I. *J. Electrochem. Soc.* **1995**, *142*, 340−347.

(49) Bar-Tow, D.; Peled, E.; Burstein, L. *J. Electrochem. Soc.* **1999**, *146*, 824−832.

(50) Eshkenazi, V.; Peled, E.; Burstein, L.; Golodnitsky, D. *Solid State Ionics* **2004**, *170*, 83−91.

(51) Andersson, A. M.; Edström, K. *J. Electrochem. Soc.* **2001**, *148*, A1100−A1109.

(52) Andersson, A. M.; Henningson, A.; Siegbahn, H.; Jansson, U.; Edström, K. *J. Power Sources* **2003**, *119*−*121*, 522−527.

(53) Leroy, S.; Blanchard, F.; Dedryvère, R.; Martinez, H.; Carré, B.; Lemordant, D.; Gonbeau, D. *Surf. Interface Anal.* **2005**, *37*, 773−781.

(54) Yazami, R. *Electrochim. Acta* **1999**, *45*, 87−97.

(55) Richard, M. N.; Dahn, J. R. *J. Electrochem. Soc.* **1999**, *146*, 2068−2077.
(56) Du Pasquier, A.; Disma, F.; Bowmer, T.; Gozdz, A. S.; Amatucci, G.; Tarascon, J. M. *J. Electrochem. Soc.* **1998**, *145*, 472−477.
(57) Abraham, D. P.; Roth, E. P.; Kostecki, R.; McCarthy, K.; MacLaren, S.; Doughty, D. H. J. *Power Sources* **2006**, *161*, 648−657.
(58) Kysar, J. W. In *Interfacial Engineering for Optimized Properties II*, 586 of Materials Research Society Symposium Proceedings, Boston, MA, Nov 27−Dec 1, 2000, p 219−230.
(59) Wang, Y. X.; Nakamura, S.; Tasaki, K.; Balbuena, P. B. *J. Am. Chem. Soc.* **2002**, *124*, 4408−4421.
(60) Wang, Y. X.; Balbuena, P. B. *J. Phys. Chem. B* **2002**, *106*, 4486−4495.
(61) Wang, Y. X.; Balbuena, P. B. *J. Phys. Chem. A* **2002**, *106*, 9582−9594.
(62) Wang, Y. X.; Balbuena, P. B. *J. Phys. Chem. B* **2003**, *107*, 5503−5510.
(63) Sun, C. H.; Lu, G. Q.; Cheng, H. M. *J. Phys. Chem. B* **2006**, *110*, 4563−4568.
(64) Jehoulet, C.; Biensan, P.; Bodet, J. M.; Broussely, M.; Moteau, C.; TessierLescourret, C. *Proc. Symp. Batteries Portable Appl. Electr. Veh.* **1997**, *97*, 974−985.
(65) Wrodnigg, G. H.; Besenhard, J. O.; Winter, M. *J. Electrochem. Soc.* **1999**, *146*, 470−472.
(66) Ein-Eli, Y.; Thomas, S. R.; Koch, V. R. *J. Electrochem. Soc.* **1997**, *144*, 1159−1165.